Hindawi
Mathematical Problems in Engineering
Volume 2020, Article ID 3914872, 11 pages
https://doi.org/10.1155/2020/3914872

Research Article

Calculation of Electric Field on Substation Equipment considering AC Ion Flow Field

Xiaoyun Tian,[1] Zhijun Lan,[1] Feng Huo,[1] Zhi Huang,[1] Shilong Huang,[2] Yujian Ding,[3] Jianghai Geng,[2] Xiaoliang Yan,[2] and Yunpeng Liu[2]

[1]*Inner Mongolia Extra High Voltage Power Supply Corporation, Huhehaote 010012, China*
[2]*Hebei Provincial Key Laboratory of Power Transmission Equipment Security Defense, North China Electric Power University, Baoding 071003, China*
[3]*China Electric Power Research Institute, Beijing 100192, China*

Correspondence should be addressed to Shilong Huang; shilong.huang@ncepu.edu.cn

Received 20 August 2020; Revised 16 November 2020; Accepted 18 November 2020; Published 3 December 2020

Academic Editor: Alessandro Lo Schiavo

With the increase of voltage levels in substation corona discharge on the surface of high voltage conductors and equipment in substations becoming more and more severe, the influence on the electromagnetic environment around substations is becoming more and more obvious. In order to study the influence of corona discharge on the ground electric field under substation equipment in AC substations, this paper proposes an improved method based on Abdel-Salam's calculation of the ion flow field on AC power lines. By redefining the criterion of corona onset and the amount of emission charge and combining with the migration, motion, and recombination of the space charge, a new model which can be applied to the calculation of AC ion flow field electric field of multiphase bundle conductors in substations is established. The calculation results of the ground power frequency electric field of the conductor at the typical tower in the light, medium, and heavy ice regions of 750 kV typical AC transmission project show that the ground electric field gradually decreases with the increase of conductor height. At the same conductor height, the ground electric field strength in the heavy ice region is the largest, while under the conductor in a light ice region, it is the smallest, and the minimum allowable conductor-to-ground distance can be concluded that the national standard limit value is not exceeded when the conductor-to-ground distance in light ice region is 24.5 m, the conductor-to-ground distance in medium ice region is 25.5 m, and the conductor-to-ground distance in heavy ice region is 26 m.

1. Introduction

With the increase of voltage levels and the expansion of the power grid scale, the electromagnetic environment problem of power transmission and transformation projects is increasingly serious. Not only will it cause certain damage to the ecological electromagnetic environment but also it will have a potential impact on human life and health. Therefore, many scholars at home and abroad have conducted extensive and in-depth research on the electromagnetic environment of power transmission and transformation projects [1–3]. The power frequency electric field around AC conductors and equipment in substations is one of the indicators to measure the severity of electromagnetic environment problems [4–6], so it is necessary to carry out systematic analysis on them. At present, scholars mainly use a method of successive image, method of moments, simulation charge method, finite element method, dipole method, and other methods to calculate the magnitude of power frequency electric field around AC electrified equipment in the substation [7–10] and emphatically analyze the influencing factors of power frequency electric field around electrified conductors from different angles such as parameters of electrified conductors, arrangement mode, height of conductors to the ground, surrounding environmental conditions, and weather conditions [11–13].

Corona discharge phenomenon produced by substation equipment in ultrahigh voltage substation under specific

environmental conditions and weather conditions will lead to the increase in power frequency electric field value around the substation, thus affecting the electromagnetic environment around the substation to a certain extent. However, there is little literature on the calculation of power frequency electric field considering the influence of corona discharge of substation equipment. When the voltage level of the substation is low, the corona discharge phenomenon has less influence on the power frequency electric field under the substation equipment, and many scholars often choose to ignore its influence on the value of the power frequency electric field when calculating. However, when the voltage level of the substation rises, the corona discharge phenomenon of the substation equipment becomes more frequent and serious. Therefore, academia generally believes that the corona discharge phenomenon should be considered when calculating the power frequency electric field around an ultrahigh voltage substation [14].

At present, the calculation of power frequency electric field under the influence of corona discharge is mainly concentrated on the live equipment in the DC system [15–18]. However, due to the time-varying characteristics of AC live equipment, space charges generated by corona discharge move back and forth around AC equipment, which increases a lot of randomness, making the calculation of AC ion flow field very difficult.

For the research on an AC ion flow field, Clade et al. calculated the AC ion flow field in corona cage early on the premise of ignoring the influence of space charge on the original electric field direction, but this method is difficult to be extended to real circuit structure [19–21]. Abdel-Salam et al. applied a simulated charge method to the calculation of ion flow field in AC circuit. Using this method, the ion flow field of the cage structure of a single-phase conductor in a laboratory was simulated and calculated, which was verified by experiments. The concept of corona charge is defined in the method, and the amount of charge emitted by the conductor is calculated. The space charge distribution is expressed as discrete line charges. The space electric field is determined by the simulation charges of the conductor itself and the space line charges and the space charges that are redistributed under the action of the space electric field. However, Abdel-Salam's method ignores the influence caused by different electric field intensities at different positions on the conductor surface, so it is not suitable for the case of uneven electric field distribution on the conductor surface such as bundle conductor and multiphase power line [22, 23].

In recent years, the calculation methods proposed are mainly based on the Salam model. Although the calculation models proposed in [24, 25] can be applied to the electric field calculation under bundle conductors and multiphase conductors in substations, assuming the electric field intensity on the conductor surface that generates corona is a fixed value in the modeling process will cause certain errors in the calculation results.

Because the corona discharge on the conductor in the UHV substation is more serious, this paper mainly studies the calculation model of the electric field considering AC ion flow field in the substation.

Moreover, the electromagnetic environment has been paid greater heed in recent years, and the Environmental Protection Administration requires that the electromagnetic environment has to be smaller than the limits prescribed in the Chinese Standards, which makes the selections of the height of conductor-to-ground stricter. Especially for the EHV AC multiphase lines, due to the high voltage level, the ground electromagnetic environment is more complex and malicious.

For the AC line, the International Commission on Nonionizing Radiation Protection (ICNIRP) stipulates that the power frequency electric field limit is 5 kV/m. The demand on the electric field limit issued by the EU in 2004 to protect workers from all kinds of material damage is also based on the ICNIRP guidelines, which provides for a maximum of 5 kV/m [26]. The national standard Code for Designing of 110 kV–750 kV Overhead Transmission Line carried out by China in 2010 provides that "with 500 kV and above transmission lines across nonpermanent residential buildings or adjacent houses, the undistorted electric field shall not exceed 4 kV/m at the housing location of 1.5 m from the ground" so as to meet the requirements of environmental protection departments [27].

Therefore, the accurate analysis of the ground electromagnetic environment is important and currently poses a key technical difficulty in the design of multiphase lines. In this paper, based on Abdel-Salam's calculation method, improvements have been made in various aspects such as judging corona onset at each point on the conductor surface and calculating the amount of the emitted charge, making it possible to calculate the flow field of AC ions near bundle conductors on multiphase lines in substations. Based on the improved model, the numerical values of the ground power frequency electric field of the conductor at a typical tower in the light, medium, and heavy ice regions of 750 kV AC transmission line project are calculated, and the variation laws of the ground electric field distribution with the conductor height under the above three different conditions are obtained.

2. Space Charge Motion Characteristics under AC Electric Field

During corona discharge of an AC conductor in a substation, the electric field changes back and forth, and the space charge is limited in the area near the conductor. Taking a single infinite cylindrical conductor arranged in parallel above the ground plane of an infinite conductor as an example, a sinusoidal voltage higher than the corona onset voltage is applied between the conductor and the ground. Then, the corona current generated by corona discharge in one AC cycle is shown in Figure 1, and the space ion motion is shown in Figure 2.

As shown in Figure 1, the AC cycle starts from point a and the voltage rises from zero. Further away from the conductor is the negative charge remaining in the negative half-cycle of the previous voltage cycle, as shown in Figure 2(a). Although the conductor voltage is 0, a small amount of negative charge induces a small electric field on

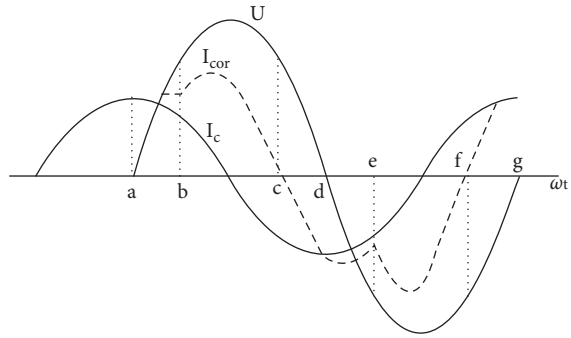

Figure 1: AC voltage and current waveform after corona initiation.

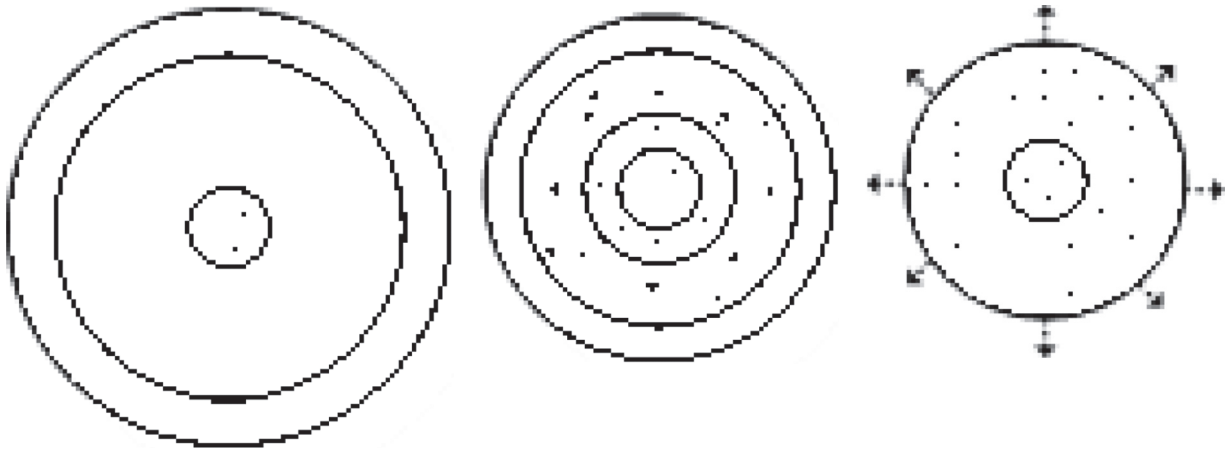

Figure 2: Schematic diagram of ion movement in half an AC cycle. (a) When the voltage is zero, the space charge distribution diagram is around the conductor. (b) Schematic diagram of space charge movement around the conductor after the corona discharge begins. (c) Schematic diagram of the space charge movement around the conductor after the corona discharge stops.

the conductor surface. Between *a* and *b*, when the conductor voltage increases, the electric field on the conductor surface and the electric field in the nearby space will increase, and the negative charge layer in the distance will accelerate to approach the conductor. At point *b*, the electric field on the conductor surface reaches the initial field strength of positive corona, and then corona discharge generates a large number of positive ions, which are far away from the conductor, while electrons rapidly approach the conductor and neutralize on the conductor surface. The residual negative ion layer continues to move towards the conductor and merges with the newly born positive ions, and a part of the negative ions are compounded with the positive ions. Most of the negative ions move to the conductor surface to neutralize. This process is shown in Figure 2(b). Positive corona discharge is maintained until point *c*, and the conductor voltage drops to an electric field higher than the corona initial field strength after the peak value. Since the presence of a large number of positive ions near the conductor weakens the surface field strength of the conductor, the conductor potential when corona stops is slightly higher than when corona starts. No positive ions are generated after the corona discharge is terminated after point *c*, and the accumulated positive charges continue to move outward. From point *c* to point *d* where the voltage is 0, the residual positive charge continues to move outward to reach the farthest distance from the conductor. After that, the voltage enters the negative half cycle. The charge movement process is similar to the positive half cycle. Corona starts at point *e* and ends at point *f*.

3. Calculation Method

The calculation method of ion flow in electric field of AC live conductors in substations proposed in this paper is improved on the basis of the Abdel-Salam method. The calculation flow is shown in Figure 3.

The AC corona loss of multiphase bundle conductors is analyzed by using the charge simulation method. First, when there is no space charge, the corona onset charge of the conductors is calculated according to the Kaptzov hypothesis (the surface field strength remains unchanged after corona onset). Then, the alternating current period

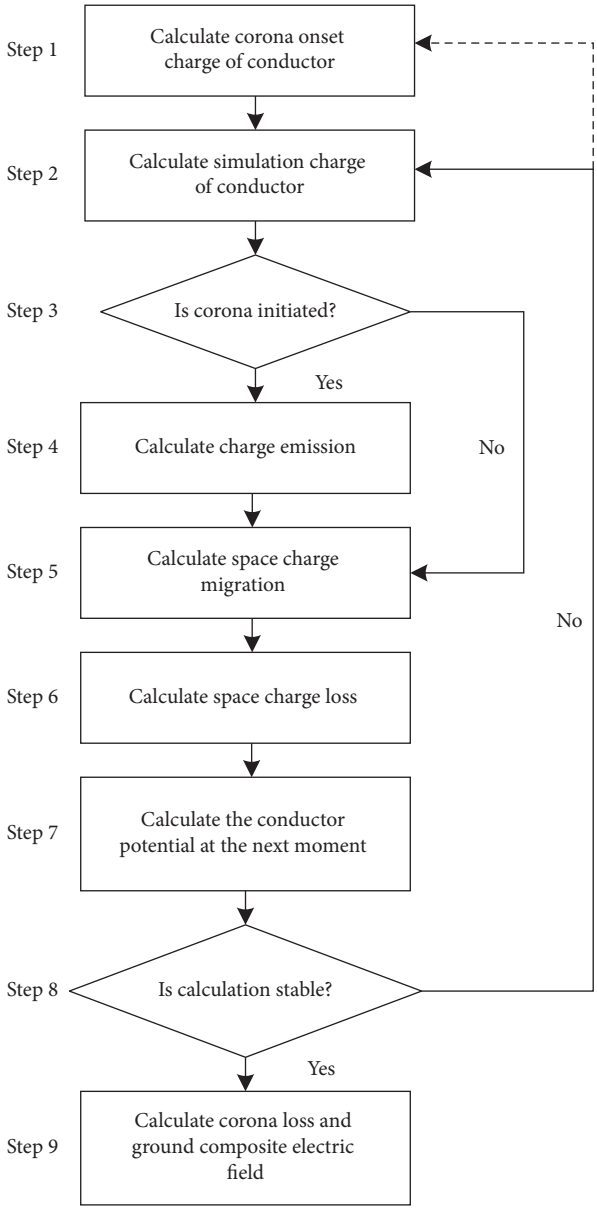

Figure 3: Flow chart of the calculation method for corona loss of AC line.

is divided into several time periods, the simulation charge quantity on the surface of the conductor is calculated at each moment and compared with the corona onset charge, and the corona onset is judged. When the corona onset occurs, the conductor emits a certain charge into space, and the space charge migrates under the action of the electric field and is combined with loss. Repeat the above steps for several AC cycles until the total charge is stable within one cycle and then stop calculation. According to the calculation results, physical quantities such as corona loss and ground electric field can be further obtained.

The improvement of the existing method in this paper is mainly in steps 1–4 in Figure 3, that is, the judgment of blooming and the determination of charge emission. Abdel-Salam's calculation methods of space charge transfer, composite loss, and corona loss are still applicable to the calculation of split conductors and multiphase lines in substations.

3.1. Calculation of Corona Charge. Kaptzov's hypothesis considers that the surface field strength remains unchanged after the corona onset. However, it is difficult to obtain the amount of charge emission on the conductor surface when the Kaptzov hypothesis is directly applied to AC line corona calculation. For this reason, Abdel-Salam introduced the concept of corona onset charge to his article. Simulation charges were uniformly set around the conductor surface. The nominal field was used to calculate the total charge amount of simulation charges when the conductor surface reached corona onset field strength, which was defined as the corona onset charge of the conductor. Assuming that the corona onset charge of the conductor does not change at each moment, it is only calculated once, and then the simulation charge of the conductor is calculated at each moment considering the current conductor potential and space charge distribution. When the total amount of simulation electric charge of the conductor exceeds the corona onset charge, the conductor is considered to be corona onset, and the excess part is evenly distributed at each point on the surface of the conductor and emitted into space.

In fact, the space charge distributed on the conductor surface will affect the electric field distribution on the conductor surface, and the corona onset charge calculated by using the nominal field cannot be guaranteed to conform to the Kaptzov hypothesis when there is space charge. On the other hand, in the asymmetric structure, the electric field distribution is uneven everywhere on the surface of the conductor, especially in the case of splitting the conductor. Using the total charge of the conductor as the corona onset criterion, it is obviously unreasonable to think that corona occurs uniformly on the surface of the conductor. In this paper, the conductor is still divided into simulation line charges, as shown in Figure 4, but the corona onset charge of the conductor is redefined as different values at various points on the surface of the conductor. It is considered that the simulation charge at a point on the surface of the conductor when the corona onset field strength is reached is the corona onset charge at that point. The effect of space charge is taken into account when calculating the corona onset charge, so the corona onset charge of the conductor must be recalculated at the beginning of each moment, as shown by the dotted line in Figure 3.

For each phase conductor, based on its radius, the corona onset field values are defined during the positive and negative half cycles of the applied AC voltage, respectively, as follows [22]:

$$E_{+\text{onset}} = \eta \times \left(33.7 + \frac{8.13}{\sqrt{R}}\right) \text{kV/cm}, \tag{1a}$$

$$E_{-\text{onset}} = \eta \times \left(31.0 + \frac{9.55}{\sqrt{R}}\right) \text{kV/cm}, \tag{1b}$$

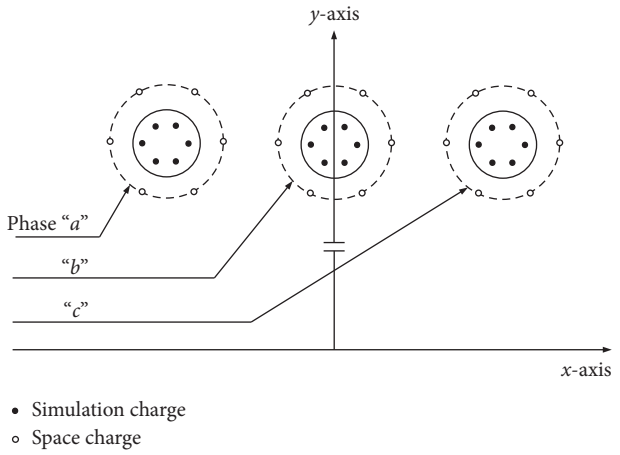

Figure 4: Schematic diagram of three transmission lines.

where R is the conductor radius in cm and η is the conductor surface factor. It is assumed that when a conductor is coronating, the conductor surface charge remains constant at the onset value. The onset field values are used to define the corresponding positive and negative onset charges for each phase conductor by solving the space-charge-free field problem.

The charge simulation technique (CST) is used to solve the space-charge-free field problem in the three-phase arrangement, as shown in Figure 4. Figure 4 shows the schematic diagram of three-phase conductor. In each phase conductor, M black-centered dots represent the simulation charge, N hollow dots represent space charge, and M matching points are uniformly selected on the surface of the conductor.

The electric field at the j^{th} match point on the conductor surface is expressed as

$$\begin{aligned}\mathbf{E}_j &= \sum_{i=1}^{3M} \frac{q_{\text{ci}}}{2\pi\varepsilon_0}\left[\frac{1}{r_{\text{ci}}}\mathbf{e}_{\text{ci}} + \frac{1}{r'_{\text{ci}}}e'_{\text{ci}}\right] + \sum_{i=1}^{3N} \frac{q_{\text{si}}}{2\pi\varepsilon_0}\left[\frac{1}{r_{\text{si}}}\mathbf{e}_{\text{si}} + \frac{1}{r'_{\text{si}}}e'_{\text{si}}\right] \\ &= \sum_{i=1}^{3M} a_{ji}q_{\text{ci}} + \sum_{i=1}^{3N} b_{ji}q_{\text{si}},\end{aligned} \tag{2}$$

where $i = 1, 2, 3, \ldots, 3M$, r_{ci} and r_{si} are the distances from the simulation charge and space charge to the matching point, respectively; r'_{ci} and r'_{si} are the distance from the corresponding image charge to the matching point; $\mathbf{e}_{\text{ci}}$ and $\mathbf{e}_{\text{si}}$ are the unit direction vectors from the simulation charge and space charge to the matching point, respectively; e'_{ci} and e'_{si} are the unit direction vectors from the corresponding image charge to the matching point; a_{ji} is the electric field coefficient of the simulation charge at the matching point; b_{ji} is the electric field coefficient of the space charge at the matching point.

For all matching points, equation (2) can be written in the following matrix form:

$$\mathbf{A}_{(3M\times 3M)}\mathbf{Q}_{\pm\text{onset}\,(3M\times 1)} + \mathbf{B}_{(3M\times 3N)}\mathbf{Q}_{s\,(3N\times 1)} = \mathbf{E}_{\pm\text{onset}\,(3M\times 1)}, \tag{3}$$

where $\mathbf{A}$ is the electric field intensity coefficient matrix of the conductor simulation charge to the matching point of the conductor; $\mathbf{B}$ is the electric field intensity coefficient matrix of space charge around the conductor to the matching point of the conductor; $\mathbf{Q}_{\pm\text{onset}}$ is the corona onset charge matrix of the conductor; $\mathbf{Q}_s$ is the space charge matrix around the conductor; and $\mathbf{E}_{\pm\text{onset}}$ is the corona onset electric field strength matrix.

According to equation (3), the amount of corona onset charge on the surface of the conductor can be calculated. The sum of all corona onset charges on the surface of each phase of the conductor is

$$\left(\mathbf{Q}_{\pm\text{onset}}\right)_a = \sum_{i=1}^{M} q_{\text{ci}}, \tag{4a}$$

$$\left(\mathbf{Q}_{\pm\text{onset}}\right)_b = \sum_{i=M+1}^{2M} q_{\text{ci}}, \tag{4b}$$

$$\left(\mathbf{Q}_{\pm\text{onset}}\right)_c = \sum_{i=2M+1}^{3M} q_{\text{ci}}, \tag{4c}$$

where the subscripts a, b, and c stand for the three phases a, b, and c, respectively, as shown in Figure 4.

3.2. Calculation of Charge Emission. Each alternation cycle is divided into NT discrete time steps. At the i^{th} time step, the instantaneous three-phase balanced applied voltages are expressed as

$$v_a = v_{\max}\sin\left(w(i-1)\Delta t\right), \tag{5a}$$

$$v_b = v_{\max}\sin\left(w(i-1)\Delta t - 120^{\circ}\right), \tag{5b}$$

$$v_c = v_{\max}\sin\left(w(i-1)\Delta t + 120^{\circ}\right), \tag{5c}$$

where $i = 1, 2, 3, \ldots, \text{NT}$. At the first time step $(i = 1)$ not all phase voltages are of zero values, as shown in Figure 5. According to equations (5a), (5b), and (5c), the three-phase voltages at the first time step are

$$v_a = 0, \tag{6a}$$

$$v_b = -0.5v_{\max}, \tag{6b}$$

$$v_c = +0.5v_{\max}, \tag{6c}$$

which means that corona may be existing on phase b and/or phase c according to the magnitude of the applied voltage and the onset field values defined by equations (1a) and (1b).

Each phase conductor is represented by M line charges in the same way as described in Section 3.1. The unknown charges are obtained by setting the potential at each matching point on each phase conductor to its respective applied voltage. The potential at any of the matching points must be calculated due to the 3M charges simulating the phase conductors and their images. The potential calculated

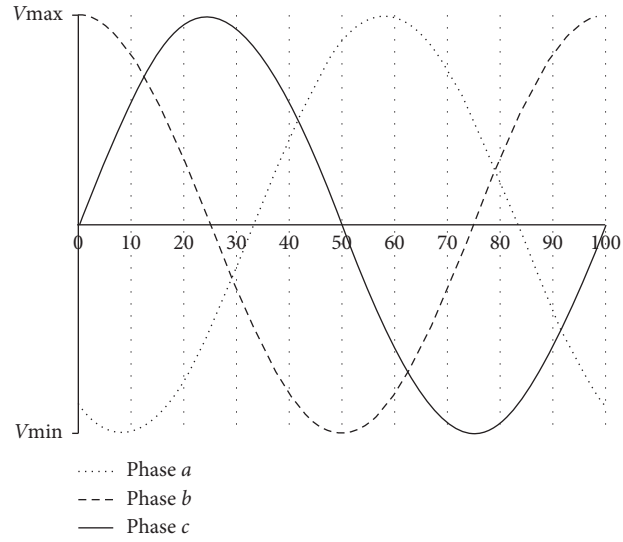

Figure 5: Three-phase balanced voltage waveform divided into 100 steps.

at the j^{th} matching point on each phase conductor is expressed as

$$v_a = \sum_{i=1}^{3M} \frac{q_{\text{ci}}}{2\pi\varepsilon_0} \ln\left[\frac{r'_{\text{ci}}}{r_{\text{ci}}}\right] + \sum_{i=1}^{3N} \frac{q_{\text{si}}}{2\pi\varepsilon_0} \ln\left[\frac{r'_{\text{si}}}{r_{\text{si}}}\right] = \sum_{i=1}^{3M} c^a_{ji} q_{\text{ci}} + \sum_{i=1}^{3N} d^a_{ji} q_{\text{si}}, \tag{7a}$$

$$v_b = \sum_{i=1}^{3M} \frac{q_{\text{ci}}}{2\pi\varepsilon_0} \ln\left[\frac{r'_{\text{ci}}}{r_{\text{ci}}}\right] + \sum_{i=1}^{3N} \frac{q_{\text{si}}}{2\pi\varepsilon_0} \ln\left[\frac{r'_{\text{si}}}{r_{\text{si}}}\right] = \sum_{i=1}^{3M} c^b_{ji} q_{\text{ci}} + \sum_{i=1}^{3N} d^b_{ji} q_{\text{si}}, \tag{7b}$$

$$v_c = \sum_{i=1}^{3M} \frac{q_{\text{ci}}}{2\pi\varepsilon_0} \ln\left[\frac{r'_{\text{ci}}}{r_{\text{ci}}}\right] + \sum_{i=1}^{3N} \frac{q_{\text{si}}}{2\pi\varepsilon_0} \ln\left[\frac{r'_{\text{si}}}{r_{\text{si}}}\right] = \sum_{i=1}^{3M} c^c_{ji} q_{\text{ci}} + \sum_{i=1}^{3N} d^c_{ji} q_{\text{si}}, \tag{7c}$$

where $i = 1, 2, 3, \ldots, 3M$ and $j = 1, 2, 3, \ldots, M$. c^a_{ji}, c^b_{ji}, and c^c_{ji} are the potential coefficients of the simulation charge at the matching point on conductors a, b, and c, respectively. d^a_{ji}, d^b_{ji}, and d^c_{ji} are the potential coefficients of the space charge at the matching point on conductors a, b, and c, respectively.

For all matching points, equation (2) can be written in the following matrix form:

$$\mathbf{C}_{(3M\times 3M)}\mathbf{Q}_{c\,(3M\times 1)} + \mathbf{D}_{(3M\times 3N)}\mathbf{Q}_{s\,(3N\times 1)} = \mathbf{V}_{\text{app}\,(3M\times 1)}, \tag{8}$$

where $\mathbf{C}$ is the potential coefficient matrix of the conductor simulation charge to the matching point of the conductor; $\mathbf{D}$ is the potential coefficient matrix of the space charge around the conductor to the matching point of the conductor; $\mathbf{Q}_c$ is the conductor simulation charge matrix; $\mathbf{Q}_s$ is the space charge matrix around the conductor; and $\mathbf{V}_{\text{app}}$ is the voltage matrix applied externally.

The solution of equation (8) evaluates the unknown charges whose summation inside each phase conductor is equivalent to its surface charge:

$$(\mathbf{Q}_c)_a = \sum_{i=1}^{M} q_{\text{ci}}, \tag{9a}$$

$$(\mathbf{Q}_c)_b = \sum_{i=M+1}^{2M} q_{\text{ci}}, \tag{9b}$$

$$(\mathbf{Q}_c)_c = \sum_{i=2M+1}^{3M} q_{\text{ci}}. \tag{9c}$$

The key to this algorithm is to calculate the surface charge emission of a conductor. In this analysis, corona onset and charge emission are, respectively, judged at each point on the conductor surface, the conductor simulation charge vector $\mathbf{Q}_c$ and corona onset charge vector $\mathbf{Q}_{\pm\text{onset}}$ are calculated at each moment, each element in the two vectors is compared, if $Q_{c,r} > Q_{+\text{onset},r}$ or $Q_{c,r} < Q_{-\text{onset},r}$, the corona onset occurs at the point r on the conductor surface, and the part $Q_{s,r} = Q_{c,r} - Q_{-\text{onset},r}$ of the simulated charge exceeding the corona onset charge is emitted into space.

3.3. Migration of Charge. Since the space line charges have the same polarity as that of the conductor, they will be repulsed away from the conductor surface under the action of the prevailing electric field. The displacements of each emitted space line charge Δx and Δy in the X- and Y-directions within a time interval Δt are

$$\Delta x = \mu E_x \Delta t, \tag{10a}$$

$$\Delta y = \mu E_y \Delta t, \tag{10b}$$

where μ is the ion mobility and was assumed constant and taken as 1.5×10^{-4} and $1.8 \times 10^{-4}\text{m}^2/\text{V}\cdot\text{s}$ for positive and negative ions. E_x and E_y are the X- and Y-components of the electric field. The electric charge emitted under the action of the electric field will move to a new position.

3.4. Loss of Charge. The space charge is pushed away or pulled closer to the conductor under the action of equations (10a) and (10b) at each moment. When a charge moves back to the conductor, it is neutralized on the surface of the conductor and disappears from the calculation.

Positive and negative charges will recombine when they meet in space. In order to calculate charge recombination, the charge density needs to be known. Here, the control volume ΔV_i of charge is defined as the fan-shaped area that the charge i passes through during the time period Δt, as shown in Figure 6. Charge density is defined as follows:

$$\rho_{\pm} = \frac{q_{\pm\text{si}}}{e\Delta V_i}, \tag{11}$$

where ΔV_i is the control volume of charge. $q_{\pm\text{si}}$ is the positive and negative line charges. e is the amount of electronic charge $e = 1.6 \times 10^{-19}\text{C}$.

After considering the recombination of positive and negative charges, the charge amount becomes

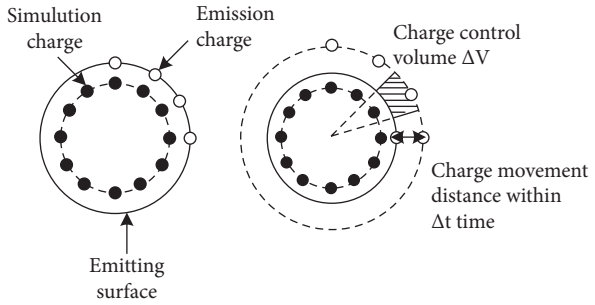

Figure 6: Schematic diagram of the charge emission process (phase a only is shown).

$$q_{\pm si,i+\Delta t} = \frac{q_{\pm si,i}}{1 + \left|\gamma \Delta t \rho_{\pm}\right|}, \tag{12}$$

where the recombination coefficient is $\gamma = 1.5 \times 10^{-12} m^2/s$ and $\rho_{\pm}$ is the positive and negative charge density.

Due to recombination, the space charge decreases continuously since it was generated. When its charge density is less than a certain value, the charge is deleted from the calculation.

3.5. Termination Criteria. Since space charges are not included in the initial conditions of the calculation, the calculation needs several cycles before it can be stabilized. The total amount of space charge record at each time is

$$q_{space,sum} = \sum_{i=1}^{3N} q_{si}. \tag{13}$$

Calculate the total amount of space charge generated in a period as follows:

$$q_{cycle,sum} = \sum_{j=1}^{N_T} q_{space,sum,j}, \tag{14}$$

where N_T is that total amount of time steps in a cycle.

It is considered that the calculation is stable when the total amount of space charge generated in two adjacent periods changes little. That is,

$$\left| \frac{q_{cycle,sum,N_c} - q_{cycle,sum,N_c-1}}{q_{cycle,sum,N_c-1}} \right| < \varepsilon, \tag{15}$$

where N_c is the current number of calculation cycles and ε is the error tolerance.

Experience shows that after 10 cycles of calculation, the error of charge amount can be controlled to less than 1%.

3.6. Calculation of Ground Electric Field. After several cycles, the calculation is stable, and the simulation charge and space charge distribution of the conductor at each moment can be obtained; thus, the electric field at any point p in space can be calculated:

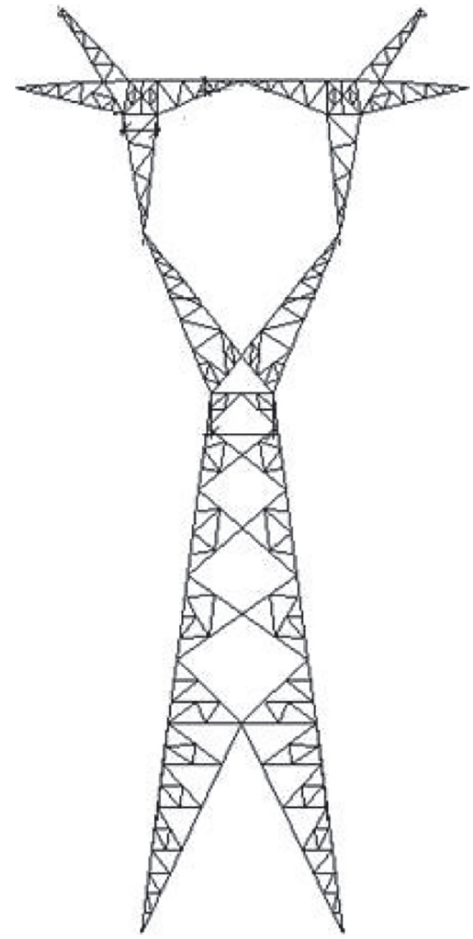

Figure 7: The typical tower type of 750 kV AC transmission line.

$$\mathbf{E}_p = \sum_{i=1}^{3M} a_{pi} q_{ci} + \sum_{i=1}^{3N} b_{pi} q_{si}, \tag{16}$$

where the first term in the right equation is the electric field generated by the conductor and the second term is the electric field generated by the space charge. a_{pi} is the electric field coefficient of the simulation charge of the conductor at point p; b_{pi} is the electric field coefficient of the space charge at point p.

4. Distribution Law of Ground Power Frequency Electric Field of AC Live Conductors

4.1. Parameter Setting. Referring to 750 kV typical AC transmission line project, the typical tower types in light, medium, and heavy ice regions are analyzed.

The typical tower type of 750 kV UHVAC transmission line is shown in Figure 7. As shown in Table 1, in light ice regions, the phase spacing is 18.2 m, and the spacing of the ground lines is 32.4 m; in medium ice regions, the phase spacing is 20.3 m, and the spacing of the ground lines is 36.1 m; in heavy ice regions, the phase spacing is 20.8 m, and the spacing of the ground lines is 33.4 m. The roughness coefficient of the conductor is set for 0.8, the altitude (m) is

Table 1: Parameter setting.

Ice regions	Conductor spacing (m)	Ground conductor spacing (m)	Roughness coefficient	Altitude (m)	Temperature (°C)	Wind speed (m/s)
Light	18.2	32.4				
Medium	20.3	36.1	0.8	2000	25	0
Heavy	20.8	33.4				

Table 2: Parameter table of the steel-cored aluminum strand.

Product model and specifications			LGJ-400/50	LGJ-460/60
Structure	Aluminum single	Number of strands/diameter (mm)	54/3.07	54/3.31
	Galvanized steel wire	Number of strands/diameter (mm)	7/3.07	7/3.31
Calculated area (mm^2)		Total	452	525
		Aluminum	400	465
		Steel	51.9	60.2

Table 3: Parameter table of galvanized steel strand.

Product model and specifications	JGJ-100	JGJ-150
Number of strands/diameter (mm)	19/2.60	19/3.20
Calculated cross-sectional area (mm^2)	100.88	152.81
Outside diameter (mm)	13.0	16.0

Table 4: Main technical parameters of OPGW.

Model	OPGW-15-120-2	OPGW-17-150-1
Area of aluminum-coated steel (mm^2)	121.1	154.8
Diameter of the outer single conductor (mm)	3.00	3.30
Type of fiber	G.652D	
Number of fiber cores	24	
Outside diameter (mm)	15.20	16.60

set for 2000, the temperature is 25°C, and the wind speed is 0 m/s.

(1) 7A2ZBC2 straight tower is selected for the light ice region, and 6 × LGJ-400/50 ACSR steel-cored aluminum strand is adopted as a conductor. One ground conductor adopts GJ-100 galvanized steel strand and the other adopts OPGW-120.

(2) The 7ZBC153 straight tower is selected for the medium ice region, and the conductor and ground conductor are the same as in the light ice region.

(3) ZBB225 straight tower and 6 × LGJ-460/60 ACSR steel-cored aluminum strand are selected for the heavy ice region. One ground conductor adopts a GJ-150 galvanized steel strand and the other adopts a OPGW-150.

The main parameters of the conductor and ground conductor are shown in Tables 1–4.

4.2. Calculation Results. For AC conductors in substations, the electric charge is limited to the vicinity of the conductors due to the alternating direction of the electric field. This part

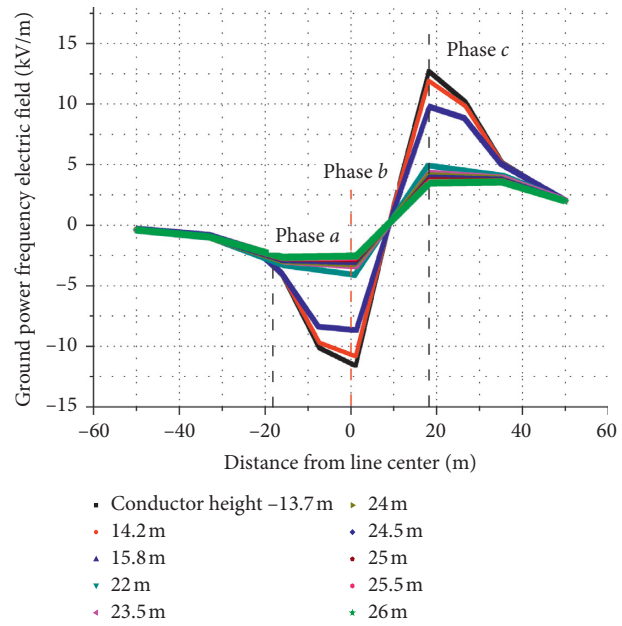

Figure 8: Distribution diagram of the ground electric field at different heights of AC conductor in light ice regions.

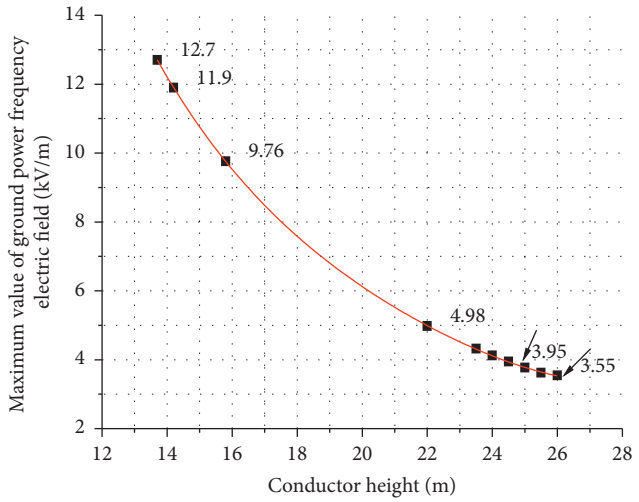

Figure 9: Variation law of the ground maximum electric field with different heights of an AC conductor in light ice regions.

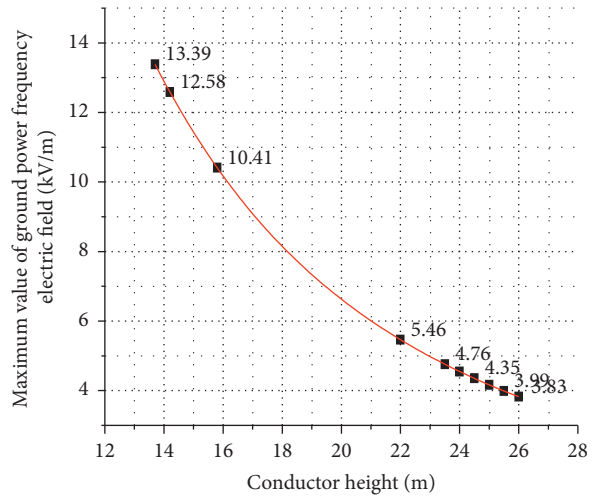

Figure 11: Variation law of the ground maximum electric field of an AC conductor with different heights in medium ice regions.

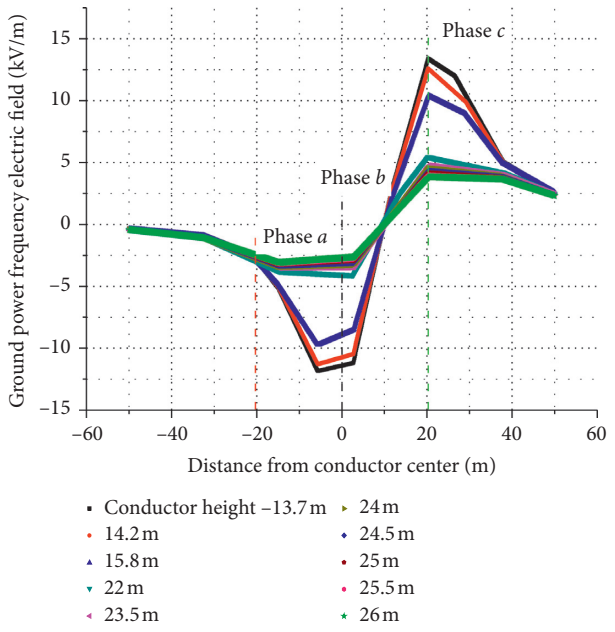

Figure 10: Distribution diagram of the ground electric field at different heights of AC conductor in medium ice regions.

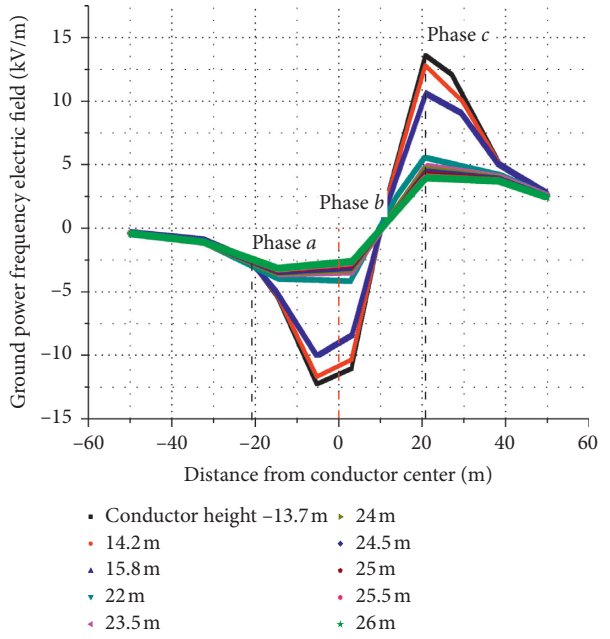

Figure 12: Distribution diagram of ground electric field at different heights of AC conductor in heavy ice regions.

mainly studies the influence of conductor height on the power frequency ground electric field. The calculation results are shown in Figures 8–13.

Figures 8, 10, and 12 show the variation of the ground electric field distribution with the conductor height when the phase C voltage reaches the positive maximum in the typical tower type in light, medium, and heavy ice regions. As the height increases, the ground electric field below the conductor decreases.

According to the national standard, when 750 kV AC overhead transmission lines pass through residential areas, the minimum conductor-to-ground distance is 19.5 m. Moreover, it needs to be satisfied that the undistorted electric field 1.5 m from the ground where the house is located shall not exceed 4 kV/m.

The following can be seen from Figures 9, 11, and 13:

(1) For light ice regions, when the conductor-to-ground distance is 24.5 m, it does not exceed the national standard limit, and the ground electric field is 3.945 kV/m.

(2) For medium ice regions, the conductor-to-ground distance is 25.5 m, which does not exceed the national standard limit, and the ground electric field is 3.991 kV/m.

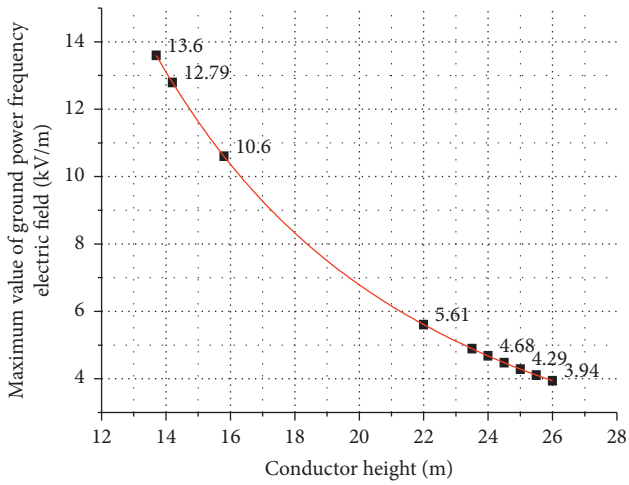

Figure 13: Variation law of the ground maximum electric field of an AC conductor with different heights in heavy ice regions.

(3) For heavy ice regions, when the conductor-to-ground distance is 26 m, it does not exceed the national standard limit, and the ground electric field is 3.940 kV/m.

If allowance is considered, the distance to the ground is higher.

5. Conclusions

(1) Based on the Abdel-Salam calculation model, this paper proposes an improved method to calculate the electric field of the ion flow field of an AC conductor in substations considering corona discharge phenomenon. Compared with the original method, the improved method is more accurate in judging the corona onset and determining the amount of emission charge and can be applied to multiphase split conductors.

(2) Using the improved method proposed in this paper, the power frequency ground electric field on the typical tower type of 750 kV AC transmission line project in light, medium, and heavy ice regions is calculated. The results show that the ground electric field gradually decreases with the increase in the line height in the three cases.

(3) According to the numerical value of the maximum electric field at different conductor heights under three conditions, it can be concluded that, under the same conductor height, the ground electric field under the conductor in the heavy ice region is the largest, and the ground electric field under the conductor in the light ice region is the smallest.

(4) According to the national standard for 750 kV AC overhead transmission lines passing through residential areas, the maximum allowable electric field strength and the minimum allowable conductor-to-ground distance can be concluded that the national standard limit is not exceeded when the conductor-to-ground distance in light ice region is 24.5 m, the conductor-to-ground distance in medium ice region is 25.5 m, and the conductor-to-ground distance in heavy ice region is 26 m.

Data Availability

The data used to support the findings of this study are available from the corresponding author upon request.

Conflicts of Interest

The authors declare that there are no conflicts of interest regarding the publication of this article.

Acknowledgments

This work was supported by the Science and Technology Project of Inner Mongolia Electric Power Group (Co., Ltd.) (issue no. NeiDianKeXin [2020] no. 29), Natural Science Foundation of China (52007063), and Fundamental Research Funds for the Central Universities (2020MS092).

References

[1] X. B. Liang, M. R. Raghuveer, and O. C. Norriselye, "Corona loss measurement on loaded operating DC lines," *IEEE Transactions on Instrument Ation and Measurement*, vol. 31, pp. 153–155, 1988.

[2] H. Kirkham, "The influence of rain rate on transmission line corona performance," *IEEE Transactions on Power Apparatus and Systems*, vol. 100, no. 1, pp. 420–430, 1981.

[3] L. X. Zhao, J. Y. Lu, and G. F. Wu, "Measurement and analysis on electromagnetic environment of 1000 kV UHV AC transmission line," in *Proceedings of the Power And Energy Engineering Conference (APPEEC)*, pp. 1023–1028, Shanghai, China, 2012.

[4] N. Trinh, P. Maruvada, and B. Poirier, "A comparative study of the corona performance of conductor bundles for 1200 KV transmission lines," *IEEE Transactions on Power Apparatus and Systems*, vol. PAS-93, no. 3, pp. 940–949, 1974.

[5] B. Y. LEE, J. K. PARK, S. H. Myung, S. W. Min, and E. S. Kim, "An effective modelling method to analyze the electric field around transmission lines and substations using a generalized finite line charge," *IEEE Transactions on Power Delivery*, vol. 12, no. 3, pp. 1143–1150, 1997.

[6] D. E. Perry, V. L. Chartier, and G. L. Reiner, "BPA 1100 kV transmission system development corona and electric field studies," *IEEE Transactions on Power Apparatus and Systems*, vol. PAS-98, no. 5, pp. 1728–1738, 1979.

[7] J. G. Andrews and A. J. Shrapnel, "Electric-field distribution around an isolated stranded conductor," *Proceeding of the Institution of Electrical Engineers*, vol. 119, pp. 1162–1166, 1972.

[8] Y. Kenichi and R. G. Olsen, "Application of a corona onset criterion to calculation of corona onset voltage of stranded conductors," *IEEE Transactions on Dielectrics and Electrical Insulation*, vol. 11, pp. 674–680, 2004.

[9] A. Yializis, E. Kuffel, and P. H. Alexander, "An optimized charge simulation method for the calculation of high voltage fields," *IEEE Transactions on Power Apparatus and Systems*, vol. PAS-97, no. 6, pp. 2434–2440, 1978.

[10] H. Singe, H. Steinbigler, and P. Weiss, "A charge simulation method for the calculation of high voltage fields," *IEEE Transactions on Power Apparatus and System*, vol. 93, pp. 1660–1668, 1974.
[11] J. H. Yu and C. Zhou, "Power-frequency electric field of EHV transmission lines under condition of complex landscape," *High Voltage Engineering*, vol. 32, pp. 18–20, 2006.
[12] H. D. Peng, W. W. Wu, Q. Hu et al., "Influence of fog water conductivity on corona discharge of AC transmission line," *High Voltage Engineering*, vol. 44, pp. 548–553, 2018.
[13] R. W. P. King, "Shielding by a house from the electric field of a power line," *Radio Science*, vol. 34, no. 4, pp. 773–779, 1999.
[14] Y. Chen, Q. F. Wan, F. Huo et al., "Corona characteristics of 1000 kV AC transmission line conductors," *High Voltage Engineering*, vol. 33, pp. 43–45+60, 2007.
[15] M. P. Sarma and W. Janischewskyj, "Analysis of corona losses on DC transmission lines: I-unipolar lines," *IEEE Transactions on Power Apparatus and Systems*, vol. PAS-88, no. 5, pp. 718–731, 1969.
[16] M. Sarma and W. Janischewskyj, "Analysis of corona losses on DC transmission lines Part II-bipolar lines," *IEEE Transactions on Power Apparatus and Systems*, vol. PAS-88, no. 10, pp. 1476–1491, 1969.
[17] X. Cui, X. X. Zhou, and T. B. Lu, "Research progress of calculation method of ion flow field in HVDC transmission line," *Proceedings of the CSEE*, vol. 32, pp. 130–141+3, 2012.
[18] W. Janischewskyj and G. Cela, "Finite element solution for electric fields of coronating DC transmission lines," *IEEE Transactions on Power Apparatus and Systems*, vol. PAS-98, no. 3, pp. 1000–1012, 1979.
[19] J. J. Clade, C. H. Gary, and C. A. Lefevre, "Calculation of corona losses beyond the critical gradient in alternating voltage," *IEEE Transactions on Power Apparatus and Systems*, vol. PAS-88, no. 5, pp. 695–703, 1969.
[20] J. J. Clade and C. H. Gary, "Predetermination of Corona losses under rain: experimental interpreting and checking of a method to calculate corona losses," *IEEE Transactions on Power Apparatus and Systems*, vol. 89, pp. 853–860, 1970.
[21] J. Clade and C. Gary, "Predetermination of corona losses under rain: influence of rain intensity and utilization of a universal chart," *IEEE Transactions on Power Apparatus and Systems*, vol. PAS-89, no. 6, pp. 1179–1185, 1970.
[22] M. Abdel-Salam and D. Shamloul, "Computation of ion-flow fields of AC coronating wires by charge simulation techniques," *IEEE Transactions on Electrical Insulation*, vol. 27, no. 2, pp. 352–361, 1992.
[23] M. Abdel-Salam and E. Z. Abdel-Aziz, "A charge simulation based method for calculating corona loss on AC power transmission lines," *Journal of Physics D: Applied Physics*, vol. 27, no. 12, p. 2570, 1994.
[24] Y. L. Zheng, J. H. Yu, Q. D. Wang et al., "Impact of corona discharge on the power frequency electric field intensity in the extra-high voltage transmission lines," *High Voltage Engineering*, vol. 35, pp. 872–876, 2009.
[25] J. H. Yu, J. Zhang, W. Q. Zhang et al., "A simple calculation method for the influence of corona discharge on the ground power frequency electric field of AC transmission line," *High Voltage Engineering*, vol. 36, pp. 1228–1233, 2010.
[26] J. Hui, Z. Guan, and Y. Liu, *High Voltage Engineering*, vol. 32, pp. 51–54, 2006.
[27] GB 50545-2010, *Code for Designing of 110 kV~750 kV Overhead Transmission Line*, p. 46, China Planning Press, Beijing, China, 2010.